








Article

Power Performance Assessment of Vertical-Axis Tidal Turbines Using an Experimental Test Rig

Aitor Fernández-Jiménez ^{1,*}, Eduardo Álvarez-Álvarez ¹, Mario López ², Mateo Fouz ³, Iván López ³, Ahmed Gharib-Yosry ⁴, Rubén Claus ² and Rodrigo Carballo ³

¹ Hydraulic R&D Group, University of Oviedo, Gonzalo Gutiérrez Quirós St, 33600 Mieres, Spain; edualvarez@uniovi.es

² DyMAST R&D Group, Department of Construction and Manufacturing Engineering, University of Oviedo, Gonzalo Gutiérrez Quirós St, 33600 Mieres, Spain; mario.lopez@uniovi.es (M.L.); clausruben@uniovi.es (R.C.)

³ Área de Ingeniería Hidráulica, University of Santiago de Compostela, Benigno Ledo St, 2, 27002 Lugo, Spain; davidmateo.fouz.varela@usc.es (M.F.); ivan.lopez@usc.es (I.L.); rodrigo.carballo@usc.es (R.C.)

⁴ Mechanical Power Department, Port Said University, Port Said 42526, Egypt; ahmed.gharib@eng.psu.edu.eg

* Correspondence: uo216958@uniovi.es

Abstract: This article presents the characteristic curves of a vertical-axis hydrokinetic tidal turbine of the Darrieus subtype aimed at meeting the electricity demand of port facilities located at harbors and estuaries with low water-speed conditions. The turbine was tested in the water-current flume of the University of Santiago de Compostela for several flow conditions with different water heights and water speeds. Blockage conditions were tested by examining the results from two groups of tests: with and without an accelerator device that restricts the flow around the rotor. The tip speed ratio and the power coefficient were used to characterize the performance of the turbine for each test. Finally, the results for open-field conditions were obtained by applying empirical expressions, which allowed us to assess the performance of the device in estuaries and harbors with known water-flow regimes.

Keywords: marine renewable energy; tidal energy; laboratory tests; tidal turbine



Citation: Fernández-Jiménez, A.; Álvarez-Álvarez, E.; López, M.; Fouz, M.; López, I.; Gharib-Yosry, A.; Claus, R.; Carballo, R. Power Performance Assessment of Vertical-Axis Tidal Turbines Using an Experimental Test Rig. *Energies* **2021**, *14*, 6686. <https://doi.org/10.3390/en14206686>

Academic Editor: Elhoussin Elbouchikhi

Received: 7 September 2021

Accepted: 12 October 2021

Published: 15 October 2021

Publisher's Note: MDPI stays neutral with regard to jurisdictional claims in published maps and institutional affiliations.



Copyright: © 2021 by the authors. Licensee MDPI, Basel, Switzerland. This article is an open access article distributed under the terms and conditions of the Creative Commons Attribution (CC BY) license (<https://creativecommons.org/licenses/by/4.0/>).

1. Introduction

Port facilities utilize a series of key services which promote the economic and social development of regions. There are a number of key activities which demand significant consumption of energy, existing important activities that demand big amounts of energy. Therefore, improvements in energy consumption are essential in order to ensure the most favorable use of electricity. It should be borne in mind that, due to their nature, there are diverse renewable hypo-carbon energies that could be used at these facilities, such as tidal currents or wave energy [1].

The total amount of energy consumed at ports represents 75% of all the energy used by the transport sector worldwide, which equates to 221 million tons of oil equivalent (MTOE) [2]. This represents 2.7% of global CO₂ emissions. Unless drastic measures are taken to reduce these emissions, it is expected that in the coming years, as a consequence of the growth of international trade, they will continue to increase, reaching 7% of all CO₂ emissions by 2040 [2].

The International Maritime Organization (IMO) has proposed different measures to reduce today's emissions by 50% up to 2050. Some such proposals include the use of renewable fuels, such as hydrogen or ammonia, or electric generation from low-carbon resources [3]. It should be noted that even some private concerns, such as the Maersk shipping company, have set a zero-emissions target for the year 2050 [4].

In the case of ports, the incorporation of electricity generation technologies from low-carbon resources will be a reality in 2030 [5]. Some examples are the port of Houston

(United States), where, in 2020, a solar panel farm was set up to supply electricity for harbor activity [6] or the port of Gothenburg (Sweden), where 80% of the electricity generated comes from a mixed plant of solar panels and windmills [7].

In this context, the development and implementation of other electric generation technologies from renewable resources, such as vertical-axis hydrokinetic turbines to harness water currents, are an excellent alternative to provide green energy to port facilities and reach the zero-emissions target set by the IMO for 2050. These devices are low-pressure turbines which generate electricity from the kinetic term (velocity) of a flowing stream with low potential energy, where the difference between upstream and downstream height is less than 0.2 m [8]. The generated energy can be used directly in the port, optimizing the environmental benefits of renewable energy, constituting a nearby point of consumption, and thereby reducing transport, operation, and maintenance costs.

The use of hydrokinetic turbines for their application in harbor areas is based on the electrical generation from the energy of tidal currents. These streams are a renewable, clean, and largely foreseeable resource which could be used to contribute to the decarbonization of port facilities. It has been estimated that tidal currents have a global energy potential of 800 TWh/year [9], meaning that their development and implementation would have a considerable niche in the world market. To date, this technology has been studied from various perspectives. These include: energy storage [10], their effects in the electrical market [11], and their economic optimization of operation [12]. Additionally, on many occasions, auxiliary mechanical elements, such as flow accelerators, need to be installed to increase velocity and ensure satisfactory operation [13].

Hitherto, the two main types of hydrokinetic turbines used to supply energy to harbor areas have been axial turbines (flow and axis parallel) and crossflow turbines (flow and axis perpendicular). Some of the real projects carried out using axial turbines include the RITE system based in New York (USA) that can generate 70 MWh/year [14] and the Kvalsund project installed in Finnmark (Norway) with a total power of 500 kW [15]. As regards crossflow rotor-based projects, the most noteworthy are the Blue Energy system settled in Canada with a total power of 2 kW [16] and the Oryon Watermill project located in the Netherlands with 150 kW of power [17], both with diameters greater than 2 m. In addition, the OceanQuest project should be highlighted, in which the testing of a 1 MW H-Darrieus prototype was carried out on the coast of Brittany (France) [18]. All of them are still in an embryonic stage, but recent results have been successful, which augers well for the future.

From a scientific point of view, the study of crossflow turbines has been based mainly on the development of numerical models. This is due to existing difficulties in the experimental characterization of these devices, such as problems with starting rotation at low water velocities and obtaining measurements of their power stage since, at these low speeds, torque is small [19]. In this sense, some studies stand out, such as the study carried out by Behroui et al. [20] where a Savonius rotor was characterized using Computational Fluid Dynamic (CFD) techniques, obtaining the mechanical performance. Another study of interest is the work of Kumar and Saini [21], which presents a numerical methodology for optimizing the blade size of a Savonius rotor taking into account the hydrodynamic parameters of the water stream.

As regards Darrieus typology, the studies presented by Kirke [22] and Benchikh Le Hocine et al. [23] stand out. Both publications considered the influence of the blockage effect on the power stage of a crossflow turbine. Thus, in the initial study, a deflector was numerically tested to observe its influence on the energy production of a rotor, while in the second publication, two numerical models were used together (CFD and Blade Element Method, BEM) to study the influence of the position of the water-free sheet on the turbine's performance.

This article presents an analysis and study of a Darrieus vertical-axis crossflow turbine in a current water flume, under blocking effects induced by a flow-accelerator device and with low water-velocity conditions (<1 m/s). The study was carried out in a water-current

flume installed in the laboratory of the Hydraulic Engineering Area at the Polytechnic School of Engineering of Lugo (University of Santiago de Compostela, USC).

2. Materials and Methods

2.1. Experimental Set-Up

A Darrieus rotor (Hydraulic R&D Group, Mieres, Spain) design was used, geometrical characteristics of which are shown in Figure 1.

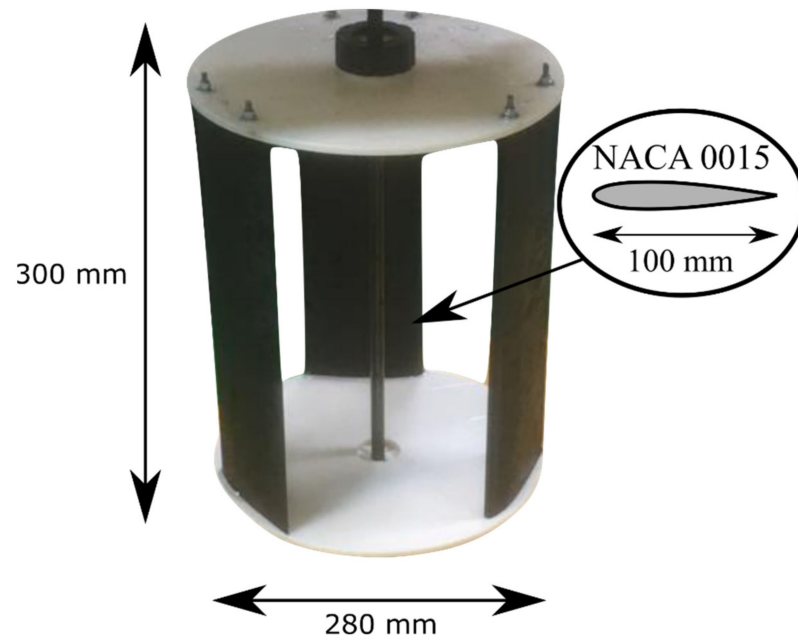


Figure 1. Darrieus rotor design tested, with the geometrical characteristics.

Using Equation (1), the solidity of this design was 0.34. This solidity value was selected because, since the rotor would work under low water-velocity conditions, having a high solidity made it easier to start the rotation of the turbine [24]. In fact, some other studies such as Singh et al. [25] and Mohammed et al. [26] show that Darrieus rotors improve their starting capacity when solidity is high since the static torque is increased, although there may be a downturn in performance.

$$\sigma = \frac{N \cdot c}{2 \cdot \pi \cdot R} \quad (1)$$

where σ is the solidity (dimensionless), N is the number of blades (dimensionless), c is the blade chord (m), and R is the rotor's radius (m).

The rotor was printed using 3D additive technology, attending to lift designs criteria to maximize performance. The material used was nylon filament (PA) due to its resistance against stresses, lightness, and non-degradation under water presence. The surface roughness of the elements that made up the rotor was reduced due to the high precision and excellent final finish of the printing equipment used (BCN3D SigmaxR19) (BCN3D, Barcelona, Spain). Additionally, after printing, the elements were subjected to sanding and sealing primer with plastic material. In consequence, the surface was completely smooth and there were no effects of turbulence in the flow due to the roughness of the turbine.

The turbine was placed in a stainless-steel metal case, in the lower part of which a radial bearing was located to ensure rotation, and the rotors were coupled to a 1.20 m-long stainless-steel shaft with a diameter measuring 10 mm. This structure was 0.62 m wide, 0.70 m long, and 1 m high, and could be found inside the water-current flume (Figure 2). In addition, two lateral windows of 0.24 m² were built so that the tests could be filmed.

The turbine was located at 0.175 m above the floor of the channel, using the lower rotor cover as a reference.

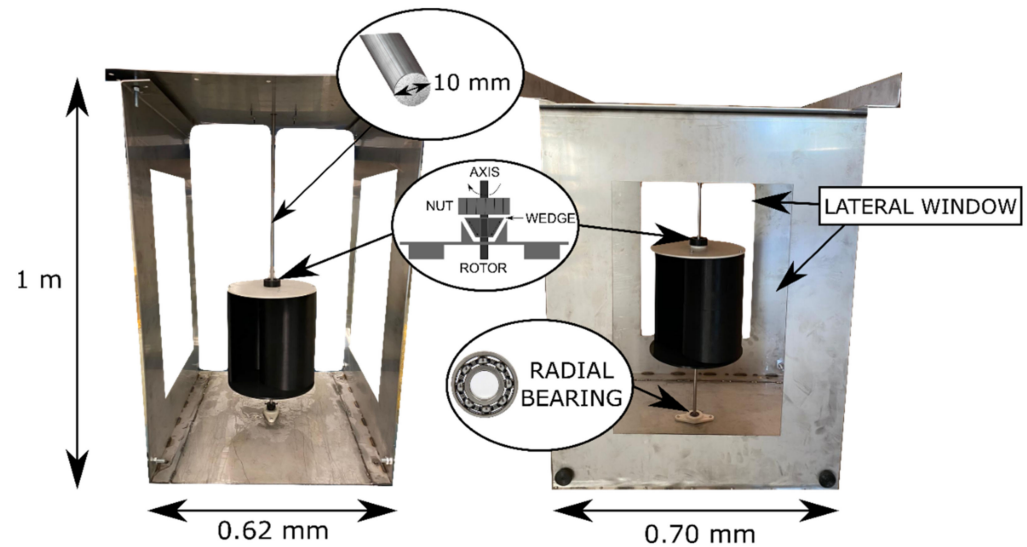


Figure 2. Structure used to couple the different rotor designs.

The structure was designed in such a way that it was possible to add and easily remove the rotor and the accelerator device by using two sets of sprats. The accelerator device was based on a symmetrical NACA profile (0015), being placed on each side of the turbine. This element allowed the incident speed to be increased by 1.6 times as the cross-section was reduced (from 0.65 m to 0.39 m). Furthermore, the use of this standardized profile for the accelerator allowed a gradual reduction in the passage section, avoiding detachments and directing the flow of water towards the rotor, minimizing the appearance of turbulent effects [27]. Figure 3 shows the accelerator device (Hydraulic R&D Group, Mieres, Spain) geometry.

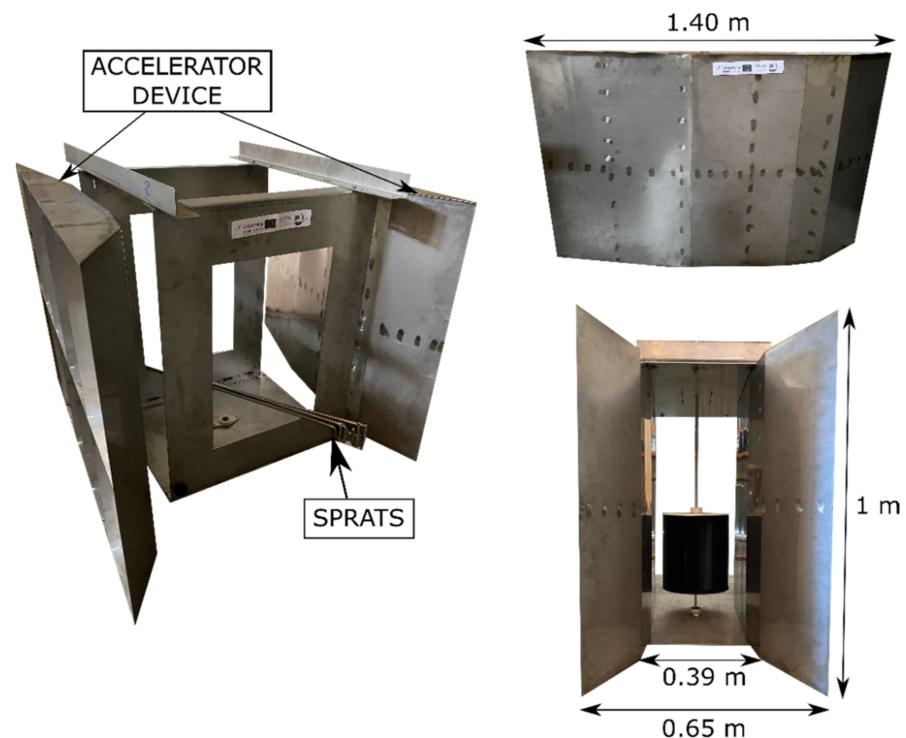


Figure 3. Geometry of the accelerator device.

A 20 m-long water-current flume, which was 0.65 m wide and 1 m high with transparent crystal walls, was used to carry out the power characterization of the selected rotor. The movement of the water inside the channel was forced by a hydraulic pump (Pedrollo Spa, San Bonifacio VR, Italy) with 22 kW of power (IDEAL-RNL-150-250/264 series). There was no free-discharge point on the circuit (Figure 4). The flow inside the channel was controlled by means of several valves that were calibrated with an ultrasonic flow meter. In this manner, different water speeds and heights could be reproduced under controlled conditions.

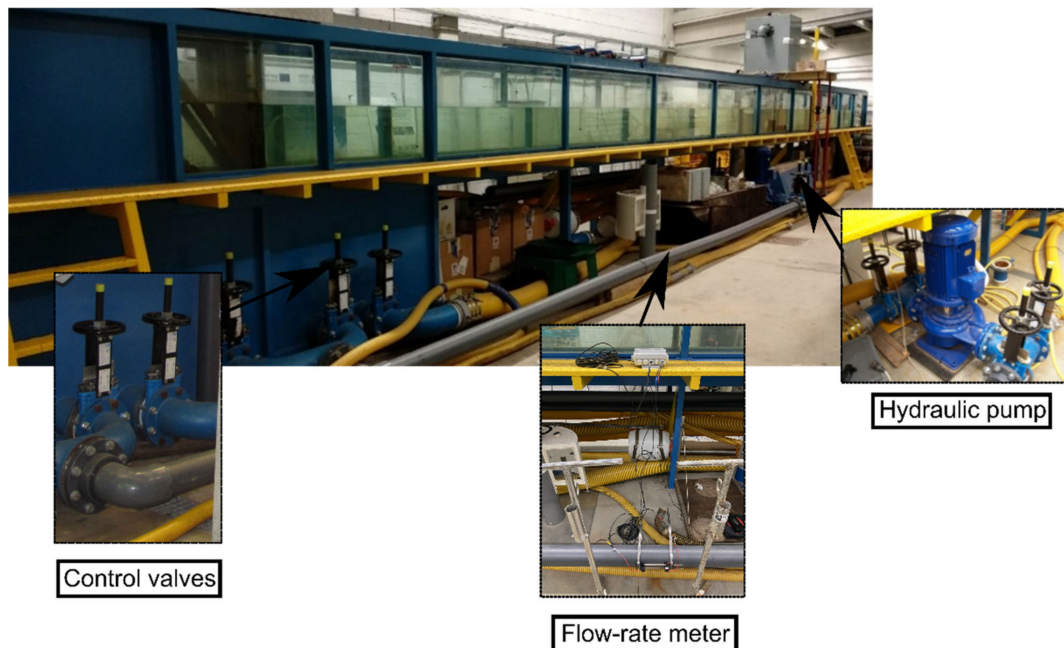


Figure 4. Water-current flume with the hydraulic control devices.

To monitor the hydraulic parameters during the tests such as flow rate, water velocity, and height variation, different sensors were used, including water-pressure devices, electric and ultrasonic water-height sensors, and an Acoustic Doppler Velocimeter (ADV) (Sontek, San Diego, CA, USA). The ADV was located just at the inlet zone of the turbine so that the speed upstream the rotor was known (Figure 5).

The power characterization simulation process of the rotor was based on variation of the resistive torque of the electric brake. In this way, for each value induced on the electric brake, a rotational speed (n) and mechanical torque (T) in the turbine were obtained, so that the rotor's power stage could be fully and satisfactorily simulated. Figure 6 shows an outline of the procedure adopted.

The characterization began with an initial measurement, called “no load”, where the electric brake did not offer resistance so that the turbine would rotate at its maximum speed but would not generate mechanical torque (Step 1). Then, by using a power-supply unit, the brake voltage was progressively varied, increasing the braking torque and obtaining, for each voltage, an n and T value of the turbine (Step 2). The test ended when the turbine stopped its rotation (Step 3).

The measurements were recorded with a high-precision torque meter (MAGTROL TS 103 series, Buffalo, NY, USA) and an electrical brake (MAGTROL HB140M series, Buffalo, NY, USA). This system measured instant torque (N·m) and rotational speed (rpm), storing and processing all data using the manufacturer's software (MAGTROL TORQUE Version 10, Buffalo, NY, USA).

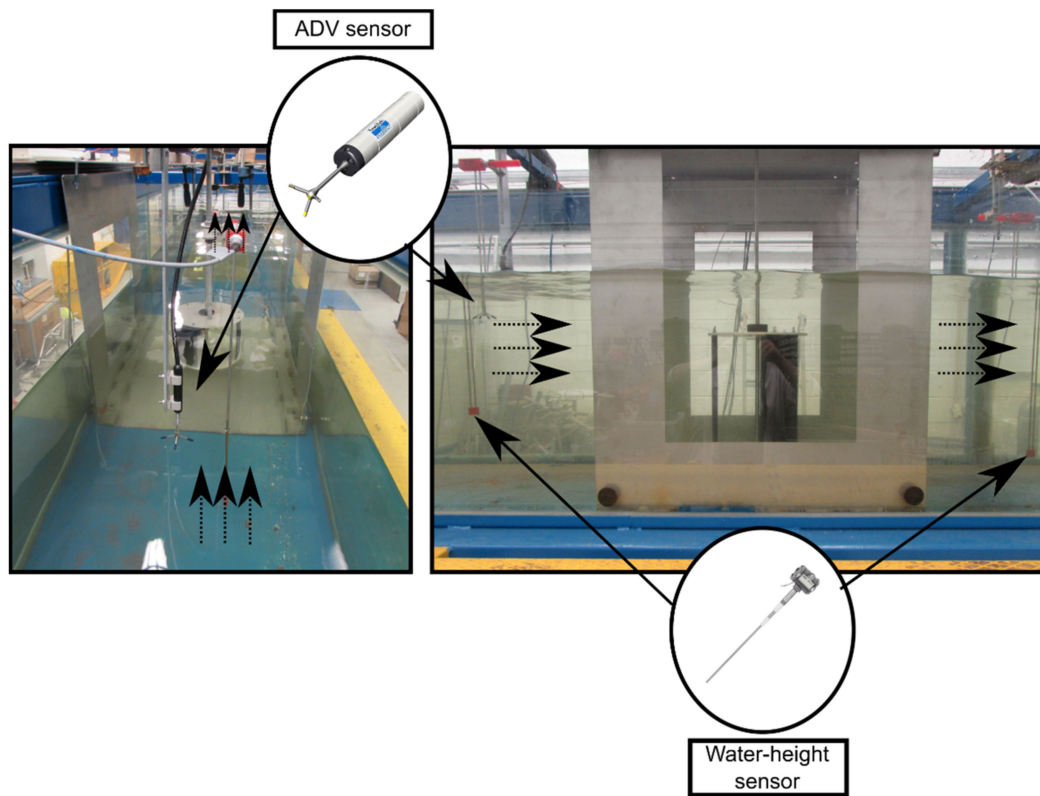


Figure 5. Hydraulic sensors' locations during tests.

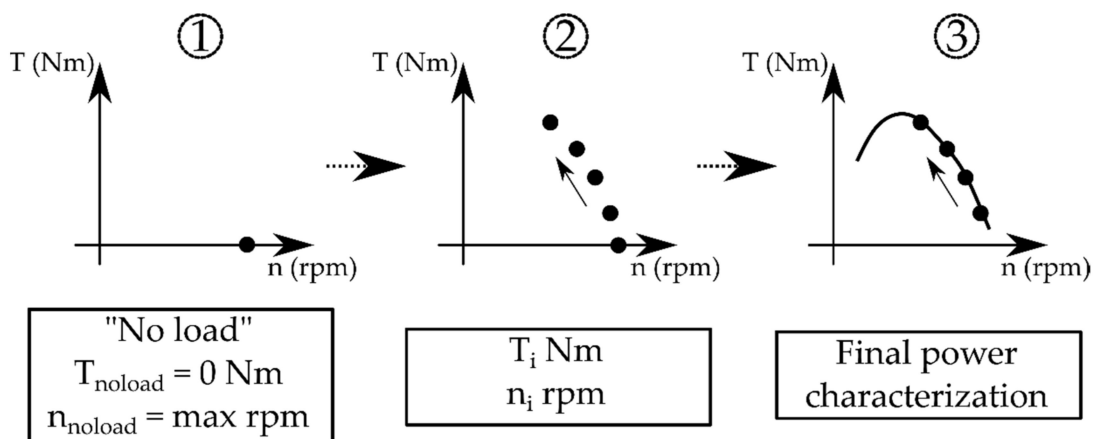


Figure 6. Scheme of the experimental characterization procedure.

2.2. Performance Indicators

The power characterization of the turbine was carried out from the raw data obtained by the torque meter. Subsequently, these data were processed, and several performance indicators were obtained. The relation of the speed at the tip of the blade with the upstream flow speed—i.e., the Tip Speed Ratio (*TSR*), was obtained by applying:

$$TSR = \frac{\omega \cdot R}{U} \tag{2}$$

with ω the rotational speed of the rotor (rad/s), and U the average water speed in the uniform zone upstream of the turbine at the channel (m/s). In addition, the power coefficient of the turbine (dimensionless) was obtained by applying:

$$Cp = \frac{P_m}{P_t} \quad (3)$$

where P_m is the average mechanical power in a complete turn of the turbine (W), obtained using:

$$P_m = \omega \cdot T \quad (4)$$

with T the torque force at the shaft (N·m), and P_t the average hydraulic power of the current during a given test (W), obtained via:

$$P_t = \frac{1}{2} \cdot \rho \cdot A_t \cdot U^3 \quad (5)$$

with ρ the fluid density (kg/m³), and A_t the area swept by the blades (m²), which was calculated by multiplying the height of the turbine (h) by the transverse width occupied by the rotor ($2R$).

2.3. Open-Field Conditions

In the presence of any blockage, the fluid is forced to pass through the rotor and the flow is accelerated [28]. This may be applied to experiments in current flumes such as those carried out in this study, but not to estuaries where the flow is unrestricted by walls near the rotor—i.e., open-field conditions. On this basis, the performance of the turbine for open-field conditions is required to assess the power production of the turbine for a possible location of interest in the vicinity of a port.

To characterize the performance of the turbine in open-field conditions, the modified values of Cp and TSR were obtained by applying:

$$Cp_F = Cp \left(\frac{U}{U_F} \right)^3 \quad (6)$$

$$TSR_F = TSR \left(\frac{U}{U_F} \right) \quad (7)$$

respectively, where U_F is the open-field flow speed corresponding to each value of water speed tested in the flume under blocked conditions (m/s). The relation between velocities, applied velocity relationship, is based on the expression proposed by Gauvin et al. [28]. This Equation (8) was selected since it performs well with blockage coefficients greater than 20%, as indicated in the case studied [28]:

$$\left(\frac{U_F}{U} \right)^2 = \frac{1}{1 - (m \cdot B)} \quad (8)$$

where B (dimensionless) is the blockage coefficient provided by:

$$B = \frac{2 \cdot R \cdot h}{b \cdot y} \quad (9)$$

with h the height of the rotor (m), b the flume width (m), y the water height at the flume (m), and m an empirical coefficient provided by [28]:

$$m = 8.14 \cdot B^2 - 7.31 \cdot B + 3.23 \quad (10)$$

A complete power characterization of the rotor was carried out to study the influence of blockage phenomena during the power stage of the turbine under low water-speed

conditions (<1 m/s). For each velocity, three water heights (0.5, 0.55, and 0.6 m) were induced with and without an accelerator device, carrying out a total of six tests. Under these conditions, values of B of 0.21, 0.23, and 0.25 were obtained for the tests without an accelerator and of 0.38, 0.41, and 0.45 when this element was placed. In both cases, the variation of blockage was made by varying the water level, although each situation was different because of changes in the hydrodynamic behavior due to the presence of the accelerator. Figure 7 shows an outline of the tests carried out.

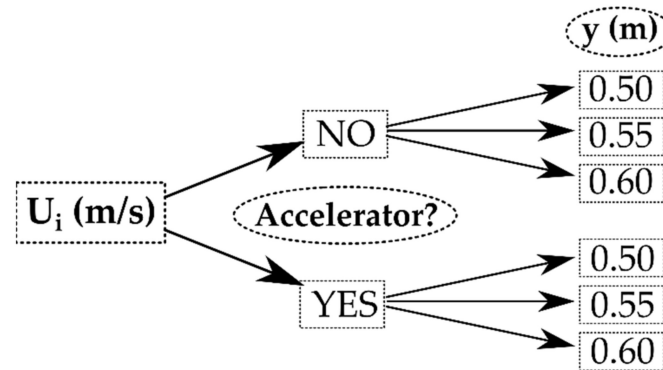


Figure 7. Outline showing how the tests were carried out.

An initial water velocity of $U_1 = 0.174$ m/s was selected because it was the cut-in speed of the rotor, while $U_3 = 0.246$ m/s was the maximum water speed of the current flume. $U_2 = 0.210$ m/s was selected as an intermediate speed. It should be noted that the position of the rotor, water-height sensors, and the ADV speed meter were invariably located in the same place during all tests. More specifically, all sensors were located at a height of 0.30 m from the bottom of the channel, and the ADV located at 0.70 m upstream of the rotor axis. Figure 8 shows a diagram with the main distances.

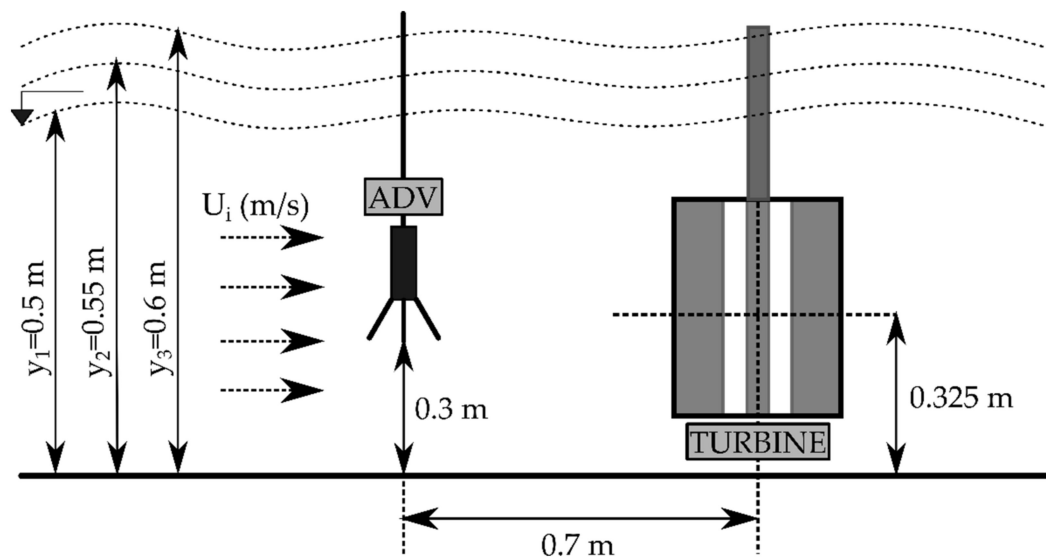


Figure 8. Diagram with the position of the different elements used in tests.

3. Results and Discussion

The proposed Darrieus water-current turbine was studied following the power characterization procedure described in previous sections. On the one hand, Figure 9 shows the variation of P_m versus the rotational speed of the turbine (n) for tests without an accelerator represented as being (a–c) whilst the different water speeds used were of 0.174, 0.210, and 0.246 m/s, respectively. On the other hand, Figure 10 shows the same tests but

using the accelerator device represented as (a–c) with water speeds of 0.174, 0.210, and 0.246 m/s, respectively.

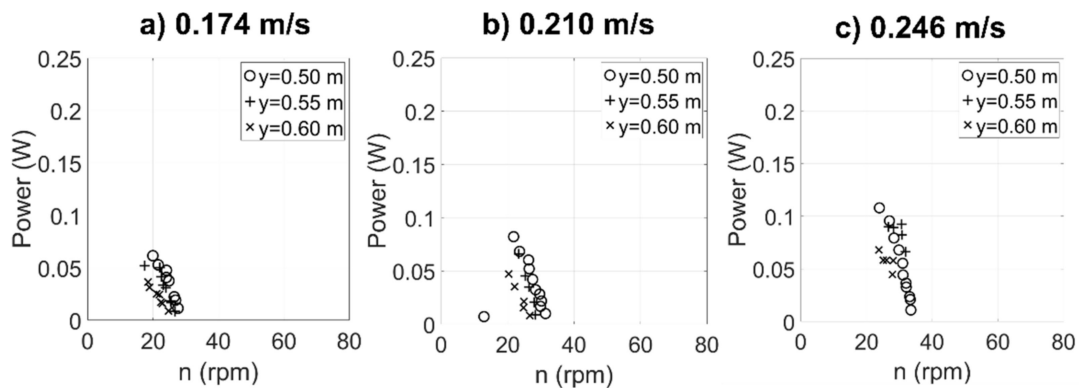


Figure 9. Variation of power vs. n for the different tests without an accelerator device.

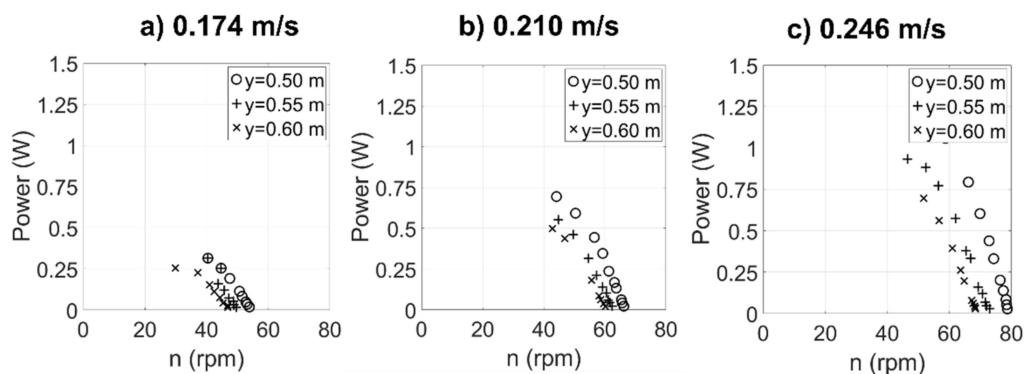


Figure 10. Variation of power vs. n for the different tests with an accelerator device.

The characteristic curves show how power values were affected by variations in the current speed and in water height. More specifically, when the current velocity increased or the water height decreased, the power of the rotor went up. This produces an increase of blockage conditions, which has direct consequences on energy extraction. In fact, the effects of blockage were noticeable when the accelerator device was installed, producing a significant increase in the rotational speed and power, even under the low water velocities of the tests.

It could also be observed how the recorded values reached a point of maximum power (maximum power point, MPP) and then the turbine stopped its rotation. The reason was that the left part of the C_p vs. TSR curve corresponds to an unstable operating zone of the turbine caused by the loss of lift force on blades (the turbine was the Darrieus NACA 0015 type that works mainly under lift forces). In the case that the rotor had a design based on drag forces (for example a Savonius type) it would be possible to obtain those points of the instability zone. [29].

Using the dimensionless coefficients of TSR and C_p it was possible to obtain an initial approximation of the operation of the designed turbine. Figure 11 shows these power parameters only with the results of the tests where the accelerator device was used since these tests conditions allow for a better visualization of the behavior of the turbine.

For the three water velocities, maximum TSR values higher than 4.5 were attained, which indicates a significant acceleration of the speed at the tip of the blade with respect to the current velocity. Furthermore, in all tests the maximum C_p values were greater than 1 due to the great blockage existing during the tests ($B > 0.38$). Therefore, it is evident that the results obtained were strongly influenced by blockage phenomenon but were not consistent with the behavior of the turbine under open-field conditions. To

obtain its characteristics without considering the blockage effects, the previously indicated Equations (6) and (7) were applied, showing in Figure 12 the C_{pF} and TSR_F values for the same tests.

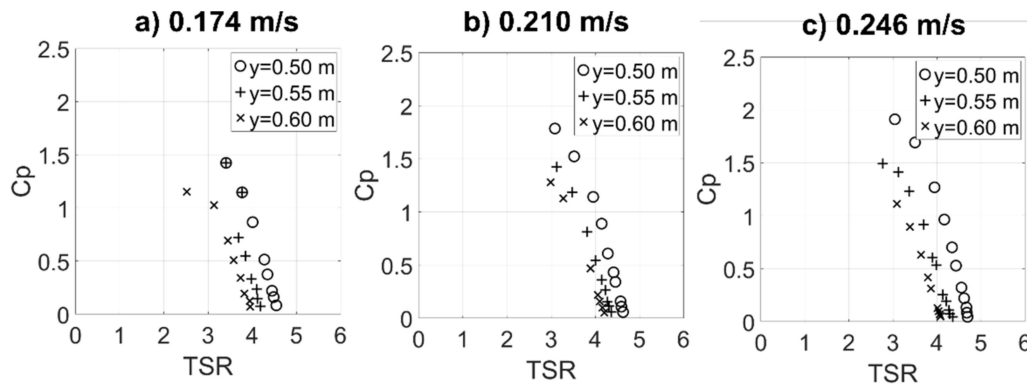


Figure 11. C_p vs. TSR curves for the three water velocities tested using the accelerator device.

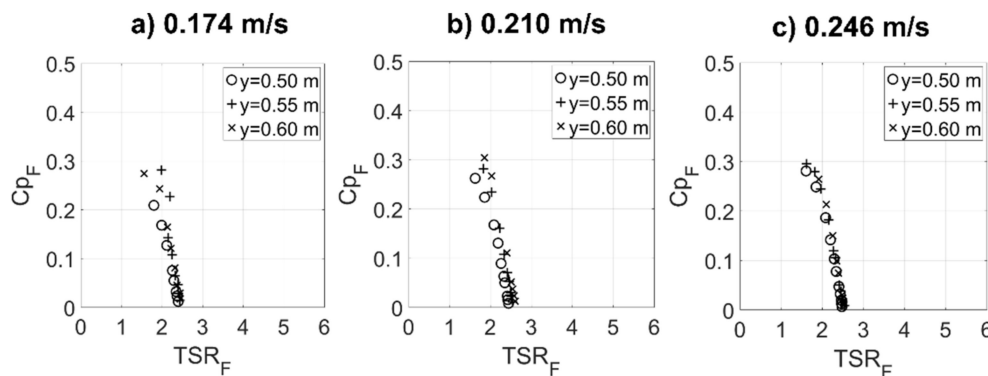


Figure 12. C_{pF} vs. TSR_F curves for the three water velocities tested using the accelerator device under open-field conditions.

The values of C_p and TSR at open-field conditions suffered a marked decrease with respect to the values under confined flow. Be that as it may, TSR values greater than 1 showed an increase in the speed at the tip of the blade, which indicates, in a preliminary way, that the rotor worked mainly at lift, so the performance of the turbine was better [21]. Further, the maximum values of C_p reached 0.29, which corresponds with more realistic values than the previous values. It should be noted that, considering the low water velocities, the turbine performed well and had good behavior due to those high-power coefficient values. Finally, and especially for the maximum water velocity, it may be observed how the characteristic curve of the turbine tended to be unique, thus eliminating the influence of the height.

4. Conclusions

In this study, the power characterization of a vertical-axis hydrokinetic tidal turbine based on the Darrieus subtype was put forward. The device under scrutiny was designed to supply electricity to port facilities located at harbors and estuaries with low water-velocity conditions. The turbine was tested in the water-current flume of the University of Santiago de Compostela to evaluate its performance under several flow conditions with three different current speeds. Moreover, the blockage effects on the performance of the turbine were examined by varying the water height and installing an accelerator device that restricted the flow around the rotor. Once the laboratory experiments were concluded, the performance of the turbine in confined and open-field conditions was satisfactorily assessed. The procurement of unrestricted results was made possible by applying empirical expressions to experimental data.

Several conclusions of interest and future research lines can be drawn from the results of this work. As expected, the power coefficient of the turbine increased when the accelerator device was installed in the water-current flume for all the flow conditions examined. This happened since blockage conditions produced changes in the water-current regime that favored the extraction of energy via by the turbine. More specifically, for the highest water velocity ($U = 0.246$ m/s) values of $C_p = 1.91$ were attained, although this result was obtained under confined flow conditions.

While the confined results were promising, open-field conditions were examined to assess the potential of this device under realistic conditions. After applying empirical expressions, C_p values decreased, reaching a maximum of 0.29 at non-restricted conditions. This result points to an excellent performance of the turbine, and possibly more, considering the low water velocities of the tests.

Future research should include the application of numerical modeling to analyze other aspects of the performance of the turbine both under blockage and open-field conditions. Furthermore, the study of flow regimes in locations of interest may be considered to assess the performance of the turbine under real conditions.

Author Contributions: Conceptualization, software, validation, investigation, resources, writing—original draft preparation, writing—review and editing, A.F.-J.; conceptualization, methodology, formal analysis, visualization, supervision, E.Á.-Á.; conceptualization, methodology, formal analysis, visualization, supervision, project administration, funding acquisition, M.L.; software, validation, investigation, resources, M.F.; software, validation, investigation, resources, I.L.; software, validation, investigation, resources, A.G.-Y.; software, validation, investigation, resources, R.C. (Rubén Claus); conceptualization, methodology, formal analysis, visualization, supervision, project administration, funding acquisition, R.C. (Rodrigo Carballo). All authors have read and agreed to the published version of the manuscript.

Funding: This research was funded by PORTOS project co-financed by the Interreg Atlantic Area Programme through the European Regional Development Fund, grant number EAPA_784/2018.

Institutional Review Board Statement: Not applicable.

Informed Consent Statement: Not applicable.

Data Availability Statement: Not applicable.

Acknowledgments: Not applicable.

Conflicts of Interest: The authors declare no conflict of interest.

References

1. Cavallaro, L.; Iuppa, C.; Castiglione, F.; Musumeci, R.; Foti, E. A Simple Model to Assess the Performance of an Overtopping Wave Energy Converter Embedded in a Port Breakwater. *J. Mar. Sci. Eng.* **2020**, *8*, 858. [CrossRef]
2. IEA. *Renewables 2020. Analysis and Forecast to 2025*; IEA: New York, NY, USA, 2020.
3. Nuchturee, C.; Li, T.; Xia, H. Energy efficiency of integrated electric propulsion for ships—A review. *Renew. Sustain. Energy Rev.* **2020**, *134*, 110145. [CrossRef]
4. Maersk. Towards a Zero-Carbon Future | Maersk. Available online: <https://www.maersk.com/news/articles/2019/06/26/towards-a-zero-carbon-future> (accessed on 4 January 2021).
5. Global Wind Energy Council. Global Wind Energy Council—GWEC: Global Wind Report 2009. 2009. Available online: <http://www.gwec.net/index.php?id=167&L=0> (accessed on 4 January 2021).
6. Port of Houston. Port Commission Approves Move on Renewable Energy | Business Wire. Available online: <https://www.businesswire.com/news/home/20191023005777/en/Port-Commission-Approves-Move-on-Renewable-Energy> (accessed on 4 January 2021).
7. Port of Gotenburg. New agreement between Swedegas and FordonsGas—Liquefied Biogas Brings Further Climate Benefits to Gothenburg Shipping | Hellenic Shipping News Worldwide. Available online: <https://www.hellenicshippingnews.com/new-agreement-between-swedegas-and-fordonsgas-liquefied-biogas-brings-further-climate-benefits-to-göthenburg-shipping/> (accessed on 4 January 2021).
8. Khan, M.J.; Bhuyan, G.; Iqbal, M.T.; Quaioco, J.E. Hydrokinetic energy conversion systems and assessment of horizontal and vertical axis turbines for river and tidal applications: A technology status review. *Appl. Energy* **2009**, *86*, 1823–1835. [CrossRef]

9. Soerensen, H.C.; Weinstein, A. *Ocean Energy: Position Paper for IPCC*; Intergovernmental Panel on Climate Change: Lubeck, Germany, 2009.
10. Bahmani-Firouzi, B.; Azizipanah-Abarghooee, R. Optimal sizing of battery energy storage for micro-grid operation management using a new improved bat algorithm. *Int. J. Electr. Power Energy Syst.* **2014**, *56*, 42–54. [[CrossRef](#)]
11. Gburczyk, P.; Wasiak, I.; Mienski, R.; Pawelek, R. Energy management system as a mean for the integration of distributed energy sources with low voltage network. In Proceedings of the International Conference on Electrical Power Quality and Utilisation, EPQU, Lisbon, Portugal, 17–19 October 2011; pp. 488–492. [[CrossRef](#)]
12. Alvarez, E.A.; Campos-Lopez, A.M.; Gutiérrez-Trashorras, A.J. OCCAM: On-line cost-function based control algorithm for microgrids. *J. Renew. Sustain. Energy* **2012**, *4*, 033101. [[CrossRef](#)]
13. Elbatran, A.H.; Ahmed, Y.M.; Shehata, A.S. Performance study of ducted nozzle Savonius water turbine, comparison with conventional Savonius turbine. *Energy* **2017**, *134*, 566–584. [[CrossRef](#)]
14. Verdant Power. Technology Evaluation of Existing and Emerging Technologies. *Water Curr. Turbines River Appl.* **2006**, *3502*, 1–48.
15. Kvalsund. Kvalsund Tidal Turbine Prototype | Tethys. Available online: <https://tethys.pnnl.gov/project-sites/kvalsund-tidal-turbine-prototype> (accessed on 4 January 2021).
16. BlueEnergy Canada INC. Blue Energy Turbine. 2020. Available online: <http://www.blueenergy.com/> (accessed on 8 January 2021).
17. Oryon. ORYON WATERMILL. Available online: <https://www.oryonwatermill.com/> (accessed on 4 January 2021).
18. “OceanQuest—HydroQuest,” 2021. Available online: <https://www.hydroquest.fr/en/oceanquest/> (accessed on 22 June 2021).
19. Espina-Valdés, R.; Fernández-Jiménez, A.; Francos, J.F.; Marigorta, E.B.; Álvarez-Álvarez, E. Small cross-flow turbine: Design and testing in high blockage conditions. *Energy Convers. Manag.* **2020**, *213*, 112863. [[CrossRef](#)]
20. Behrouzi, F.; Nakisa, M.; Maimun, A.; Ahmed, Y.M.; Souf-Aljen, A.S. Performance investigation of self-adjusting blades turbine through experimental study. *Energy Convers. Manag.* **2019**, *181*, 178–188. [[CrossRef](#)]
21. Kumar, A.; Saini, R. Performance parameters of Savonius type hydrokinetic turbine—A Review. *Renew. Sustain. Energy Rev.* **2016**, *64*, 289–310. [[CrossRef](#)]
22. Kirke, B. Tests on ducted and bare helical and straight blade Darrieus hydrokinetic turbines. *Renew. Energy* **2011**, *36*, 3013–3022. [[CrossRef](#)]
23. Le Hocine, A.E.B.; Lacey, R.J.; Poncet, S. Multiphase modeling of the free surface flow through a Darrieus horizontal axis shallow-water turbine. *Renew. Energy* **2019**, *143*, 1890–1901. [[CrossRef](#)]
24. Yosry, A.G.; Fernández-Jiménez, A.; Álvarez-Álvarez, E.; Marigorta, E.B. Design and characterization of a vertical-axis micro tidal turbine for low velocity scenarios. *Energy Convers. Manag.* **2021**, *237*, 114144. [[CrossRef](#)]
25. Singh, M.; Biswas, A.; Misra, R. Investigation of self-starting and high rotor solidity on the performance of a three S1210 blade H-type Darrieus rotor. *Renew. Energy* **2015**, *76*, 381–387. [[CrossRef](#)]
26. Chong, W.T.; Muzammil, W.K.; Wong, K.H.; Wang, C.-T.; Gwani, M.; Chu, Y.J.; Poh, S.-C. Cross axis wind turbine: Pushing the limit of wind turbine technology with complementary design. *Appl. Energy* **2017**, *207*, 78–95. [[CrossRef](#)]
27. Sarraf, C.; Djeridi, H.; Prothin, S.; Billard, J. Thickness effect of NACA foils on hydrodynamic global parameters, boundary layer states and stall establishment. *J. Fluids Struct.* **2010**, *26*, 559–578. [[CrossRef](#)]
28. Gauvin-Tremblay, O.; Dumas, G. Two-way interaction between river and deployed cross-flow hydrokinetic turbines. *J. Renew. Sustain. Energy* **2020**, *12*, 034501. [[CrossRef](#)]
29. Álvarez-Álvarez, E.; Rico-Secades, M.; Fernández-Jiménez, A.; Espina-Valdés, R.; Corominas, E.L.; Calleja-Rodríguez, A.J. Hydrodynamic water tunnel for characterization of hydrokinetic microturbines designs. *Clean Technol. Environ. Policy* **2020**, *22*, 1843–1854. [[CrossRef](#)] [[PubMed](#)]